

# Altimeter Observation of Wind-Wave-Current Interaction in the Kuroshio and Regional Impact

Paul A. Hwang

Remote Sensing Division, Naval Research Laboratory, Washington DC, USA

## Abstract

Kuroshio is the major ocean current conveying heat and mass in the Pacific Ocean. In this paper, the impact of Kuroshio on regional wind speed and wave height is studied with spaceborne altimeter measurements in the Yellow and East China Seas. In this area the Kuroshio trajectory is relatively stationary and the monsoon pattern dominates, making the region an ideal nature's laboratory for large scale air-sea-current interaction research. Major findings from the present analysis include: (a) The Kuroshio exerts significant influence on the wind and wave distributions over a swath of about 800 km wide along its path. (b) The seasonal average wind speed typically reaches maximum near the Kuroshio axis. The magnitude of enhancement due to Kuroshio ranges between 30 and 50 percent. A similar level of enhancement in the average wave height is observed. The Kuroshio effects on wave heights are further complicated by the hydrodynamic modulation of wave-current interaction and stability effects on wind wave generation. (c) Kuroshio effects are most prominent in the first and last quarters of the year, and least prominent in the third quarter.

Key word: Wind wave current interaction, Kuroshio, Modulation

## I. Introduction

Spaceborne altimeters provide measurements of wind speed,  $U_{10}$ , and significant wave height,  $H_s$ , at intervals of about 7 km along the satellite ground tracks. Comparison studies of altimeter measured wind speed and wave height with surface buoy data show excellent agreement (e.g., Freilich and Challenor, 1994; Gower, 1996; Hwang et al., 1998). The synoptic data can be used to produce seasonal and annual wind and wave climatologies to one-degree resolution (Hwang and Teague, 1998) and to investigate the spatial patterns of wind and wave distributions in regional scales. Synoptic pictures of the seasonal climatology of winds and waves constructed from the TOPEX data display considerable details of spatial structures (Hwang and Teague, 1998). One of the most interesting features related to this study is the local intensification of the wind speed and wave height along the Kuroshio axis. Examinations of the wind and wave distributions along ground tracks crossing the Kuroshio or the Gulf Stream in other regions do not show similarly distinctive enhancements. It is assumed that for such feature to manifest in measurements, a stable path of the major ocean currents is required. The Kuroshio in the East China Sea (ECS) is confined by bathymetry (Sun and Su, 1994; Qiu and Imasato, 1990; Lie et al., 1998). The seasonal locations of the Kuroshio axes in the ECS based on geomagnetic electrokinetograph (GEK) surveys (Sun and Su, 1994) are plotted in Fig. 1a. The relatively stable course of the Kuroshio and the regular monsoon weather patterns make the region a nature's laboratory for investigating regional scale air-sea-current interactions. This article is an excerpt of an earlier publication on the analysis of the effects of Kuroshio on

wind and wave conditions in the ECS region (Hwang, 2005).

## II. Analysis

To evaluate the quantitative effects of the Kuroshio modulation of regional wind and wave properties, the data from individual satellite ground tracks provide the highest spatial resolution. In this study, ground track 69, which passes through the central portion of the region (Fig. 1a), is selected for detailed investigation. Examples of the cycle-by-cycle spatial distributions of  $H_s$  and  $U_{10}$  along ground track 69 can be found in Fig. 4 of (Hwang et al., 1999). The seasonal average of wind and wave distributions derived from the altimeter data reflects the climatology of the region. In the winter, the Mongolian high pressure system dominates the geostrophic winds and forms an anticyclonic gyre in the region. The primary wind direction in the winter months is northerly in the Yellow Sea (YS) and northeasterly in the ECS. During the summer, the Indian Ocean low pressure system dominates, creating a cyclonic gyre in the region. The wind direction is southerly to southeasterly in the whole region. During the transitional seasons between the two dominant weather systems the winds fluctuate (Wang and Aubery, 1987). The seasonal distributions of  $H_s$  and  $U_{10}$  along ground track 69 are shown in Fig. 1b-c. The Kuroshio crosses ground track 69 at approximately 28°N (Fig. 1a). The wind and wave distributions show distinctive enhancement in the neighborhood of the Kuroshio. The effect is especially strong in Q1 (January, February and March) and Q4 (October, November and December). For these two quarters, the wind speed distributions in the region north of 32°N are relatively constant except near the coastal region (Fig. 1c).

South of 32°N in the ECS, seasonal wind speed distribution increases steadily at a rate of 0.3 to 0.4 m/s per degree latitude between 29 to 32°N. Within approximately 100 km of the Kuroshio axis, the growth rate increases significantly, ranging from 0.7 to 1.2 m/s per degree latitude. After passing the Kuroshio axis, wind speed decreases at a comparable rate of -1 to -1.4 m/s per degree latitude. Modulation effect on the south side of Kuroshio is disrupted by the Ryukyu Island chain at about 27°N. Q2 (April, May and June) is the transitional season and the magnitudes of  $U_{10}$  and  $H_s$  are much smaller than their counterpart in Q1 and Q4. The level of modulation, however, is comparable to Q1 and Q4. In Q3 (July, August and September) when southerly monsoon prevails in the region, a similar but smaller local enhancement in the wind speed distribution is also apparent, but the overall distribution is more irregular compared to that of the other three seasons. The multiple peaks pattern revealed in the Q3 wind speed distribution suggests additional sources of warm water near 31° and 32.5°N in the third quarter. These features match the Yangtze Bank Ring Front observed from satellite sea surface temperature data (Hicox et al., 2000). Overall, the maximum wind speed near the Kuroshio core is about 30 to 50 percent higher than that outside the range of influence (about north of 32°N). The seasonal average of wave heights has many similarities with the seasonal wind speed distribution, except that in the region of constant wind speed north of 32°N and away from coastal influence, wave continues to increase due to fetch growth (Fig. 1b).

One of the obvious mechanisms producing the observed local enhancement of wind speeds is the unstable atmospheric boundary layer above the Kuroshio Current. Intuitively, the instability generates vertical convection in the vicinity of the Kuroshio. The vertical convection in turn enhances horizontal air flow due to fluid continuity. Based on the results shown in Fig. 1c, the region of immediate influence of the Kuroshio on the wind speed distribution is about 100 km on either side of the Kuroshio axis, and the extended influence may reach 400 km from the core. The Kuroshio effects on the region's atmospheric and oceanographic climatology are obviously quite far-reaching and cover a swath of about 800 km along its path.

Near the immediate neighborhood of the Kuroshio axis, additional enhancement of winds and waves is apparent. The wave height enhancement upstream and the subsequent decrease downstream of the Kuroshio axis is a characteristic feature of surface wave modulation by current shear (Longuet-Higgins and Stewart, 1960; Keller and Wright, 1975; Thompson and Gasparovic, 1986; Hwang and Shemdin, 1990; Hwang, 1999). The wave action density conservation equation can be used to quantify the current modulation of surface waves,

$$\frac{dN}{dt} = \frac{\partial N}{\partial t} + \frac{\partial N}{\partial \vec{x}} \frac{\partial \vec{x}}{\partial t} + \frac{\partial N}{\partial \vec{k}} \frac{\partial \vec{k}}{\partial t} = \sum S_i, \quad (1)$$

where  $N$  is the wave action,  $t$  is time,  $\vec{x} = (x, y)$  is the space vector,  $\vec{k} = (k_1, k_2)$  is the wavenumber vector, and  $S_i$  are source terms. The partial differential equation (1) can be transformed into a system of ordinary differential equations,

$$\frac{dN}{dt} = \sum S_i, \quad (2)$$

$$\frac{d\vec{x}}{dt} = \vec{c}_g + \vec{U}, \quad (3)$$

$$\frac{d\vec{k}}{dt} = -k_1 \nabla U - k_2 \nabla V, \quad (4)$$

where  $\vec{c}_g$  is the group velocity, and  $\vec{U} = (U, V)$  is the current vector. Eqs. (2-4) can be solved by the method of characteristics (Hughes, 1978; Thompson and Gasparovic, 1986; Hwang and Shemdin, 1990). For the Kuroshio modulation of wind-generated waves, assume an 1D Gaussian current profile,

$$U(y) = U_0 \exp\left[-\left(\frac{y}{y_b}\right)^2\right], \quad (5)$$

where  $U_0$  is the peak current velocity at the core, and  $y_b$  is a scale width of the current. An example of the current profile  $U(y)$ , current shear  $U_y(y)$ , and the resulting modulation of the wave spectral density is shown in Figs. 2a-c. For these examples,  $U_0=1$  and 2 m/s,  $y_b=50$  km, the initial (unperturbed) wavenumber is  $k_0=0.1$  rad/m, and the wave is propagating toward -140° relative to the current axis (0° is toward downstream). Additional calculations for different values of  $U_0$ ,  $k_0$ , and wave propagation angles produce similar modulation results. Fig. 2d shows the computed modulation level as a function of angle between wave and current for three combinations of peak current speeds and wavenumbers. In Fig. 2c, field data from Q1 and Q4 are superimposed on the computed curves. From this figure, several observations can be made: (a) The directional response of the wave modulation by surface current is sinusoidal, with minimal modulation in the cross current orientation. Wave propagating at a shallow angle in the current direction (near 0°) can be refracted back and unable to cross the current (Wang et al., 1994). (b) The amplitude response is linearly proportional to the peak current velocity. And (c) the modulation level increases with wavenumber for a given current strain. All these are in accordance with the relaxation theory of wave-current interaction<sup>11-16</sup>. The maximum modulation level due to hydrodynamic straining for winter conditions, with the wave vector at -120° to -180° relative to the Kuroshio axis, is about 10 to 20 percent assuming that the peak velocity of the Kuroshio is between 1 and 2 m/s. The observed Kuroshio enhancement

is about 20 to 40 percent (Fig. 2c). The additional impact can be attributed to the unstable stratification created by the warm current. The growth rate of wind wave generation under unstable stratification has been observed to be more than double the growth rate in neutral conditions (Kahma and Calkoen, 1994; Young, 1999). The hydrodynamic modulation contributes about 25 to 50 percent of the observed Kuroshio enhancement shown in Figs. 1b and 2c.

### III. Summary

The Kuroshio is the major ocean current conveying heat and mass in the Pacific Ocean. It plays a role similar to the Gulf Stream in the Atlantic Ocean. In the East China Sea, the Kuroshio trajectory is relatively stationary, the monsoon patterns dominate, and the boundaries are well defined, making the region an ideal natural laboratory for large scale air-sea-current interaction research. The impact of the Kuroshio on winds and waves has been studied using spaceborne altimeter data. The results show that the Kuroshio exerts a significant influence on winds and waves over a swath about 800-km wide along its path, and increases the average  $U_{10}$  by about 20 to 50 percent. The Kuroshio modulations of winds and waves are most prominent in the first and fourth quarters when air-sea temperature contrast is high. In the second and third quarters, when the Kuroshio influence weakens, effects from regional frontal structures become more detectable.

The wave-height distributions display similar patterns to those of the wind-speed distributions. The magnitude of the wave-height enhancement is larger than that attributable to the wind-speed enhancement. In addition to the unstable thermal stratification, it is suggested that the wave-current interaction is another important mechanism boosting the wave-height enhancement. Numerical computations using the action density conservation equation show that the contribution due to wave-current interaction is on the same level as the direct effect of the wind-speed enhancement.

### IV. References

- Freilich, M. H. & Challenor, P. G. A new approach for determining fully empirical altimeter wind speed model functions. *J. Geophys. Res.* **99**, 25051-25062 (1994).
- Gower, J. F. R. Intercomparison of wave and wind data from TOPEX/POSEIDON. *J. Geophys. Res.* **101**, 3817-3829 (1994).
- Hickox, R., Belkin, I., Cornillon, P., and Shan, Z. Climatology and seasonal variability of ocean fronts in the East China, Yellow and Bohai Seas from satellite SST data. *Geophys. Res. Lett.* **27**, 2945-2948 (2000).
- Hughes, B. A. The effect of internal waves on surface wind waves, 2. Theoretical analysis. *J. Geophys. Res.* **83**, 455-465 (1978).
- Hwang, P. A. Microstructure of ocean surface roughness: A study of spatial measurement and laboratory investigation of modulation analysis. *J. Atmos. Ocean. Tech.* **16**, 1619-1629 (1999).
- Hwang, P. A. Altimeter measurements of the wind and wave modulation by the Kuroshio in the Yellow and East China Seas. *J. Oceanogr.*, **61**, 987-993 (2005).
- Hwang, P. A. & Shemdin, O. H. Modulation of short waves by surface currents - a numerical solution. *J. Geophys. Res.* **95**, 16311-16318 (1990).
- Hwang, P. A., Teague, W. J., Jacobs, G. A. & Wang, D. W. A statistical comparison of wind speed, wave height and wave period derived from satellite altimeters and ocean buoys in the Gulf of Mexico region. *J. Geophys. Res.* **103**, 10451-10468 (1998).
- Hwang, P. A. & Teague, W. J. Technical evaluation of constructing wind and wave climatologies using spaceborne altimeter output, with a demonstration study in the Yellow and East China Seas. *Naval Research Laboratory Memo. Rep. NRL/MR/7332-98-8216*, 41 pp (1998).
- Hwang, P. A., Bratos, S. M., Teague, W. J., Wang, D. W., Jacobs, G. A. & Resio, D. T. Winds and waves in the Yellow and East China Seas: Spaceborne altimeter measurements and model results. *J. Oceanogr.* **55**, 307-325 (1999).
- Kahma, K. K. & Calkoen, C. J. Reconciling discrepancies in the observed growth of wind-generated waves. *J. Phys. Oceanogr.* **22**, 1389-1405 (1992).
- Keller, W. C. & Wright, J. W. Microwave scattering and the straining of wind-generated waves. *Radio Sci.* **10**, 135-147 (1975).
- Lie, H.-J., Cho, C.-H., Lee, J.-H., Niiler, P. & Hu, J.-H. Separation of the Kuroshio water and its penetration onto the continental shelf west of Kyushu. *J. Geophys. Res.* **103**, 2963-2976 (1998).
- Longuet-Higgins, M. S. & Stewart, R. W. Changes in the form of short gravity waves on long waves and tidal currents. *J. Fluid. Mech.* **8**, 565-583 (1960).
- Qiu, B. & Imasato, N. A numerical study on the formation of the Kuroshio Counter Current and the Kuroshio Branch Current in the East China Sea. *Cont. Shelf Res.* **10**, 165-184 (1990).
- Sun, X.-P., and Su, Y.-F. On the variation of Kuroshio in East China Sea, *Oceanology of China Seas*, eds. Zhou, D., Y.-B. Liang, and C. K. Zeng, Kluwer Academic Press, 49-58 (1994).
- Thompson, D. R. & Gasparovic, R. F. Intensity modulation in SAR images of internal waves. *Nature* **320**, 345-348 (1986).
- Wang, Y. & Aubrey, D. G. The characteristics of China coastline. *Cont. Shelf Res.* **7**, 329-349 (1987).
- Wang, D.W., Liu, A. K., Peng, C. Y. & Meindl, E. A. Wave-current interaction near the Gulf Stream during the Surface Wave Dynamics Experiment. *J. Geophys. Res.* **99**, 5065-5079 (1994).
- Young, I. R. *Wind generated ocean waves*. Elsevier, Amsterdam, the Netherlands, 288 pp (1999).

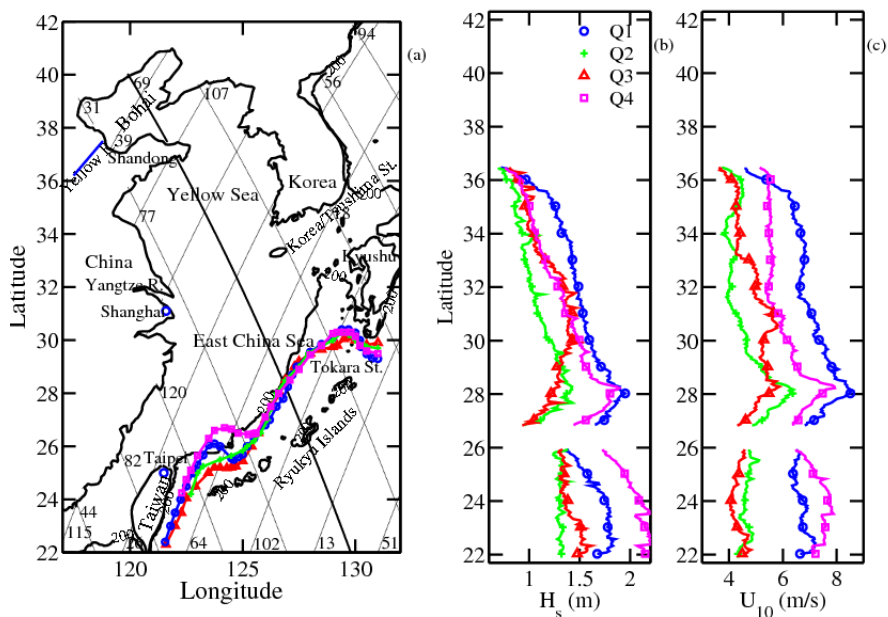


Figure 1. Modulation of winds and waves by the Kuroshio. (a) TOPEX ground tracks in the Yellow and East China Seas region, with track 69 highlighted. The seasonal variation of the Kuroshio axes are superimposed on the map (+: spring,  $\Delta$ : summer,  $\square$ : fall,  $\circ$ : winter). The 200 m depth contour is also shown. Seasonal average of (b) wave height and (c) wind speed along ground track 69. The results are based on four years average (1993-1996) of TOPEX outputs. The Kuroshio axes intersect ground track 69 at approximately 28°N. Local enhancement of wind speed and wave height is attributed to the Kuroshio influence.

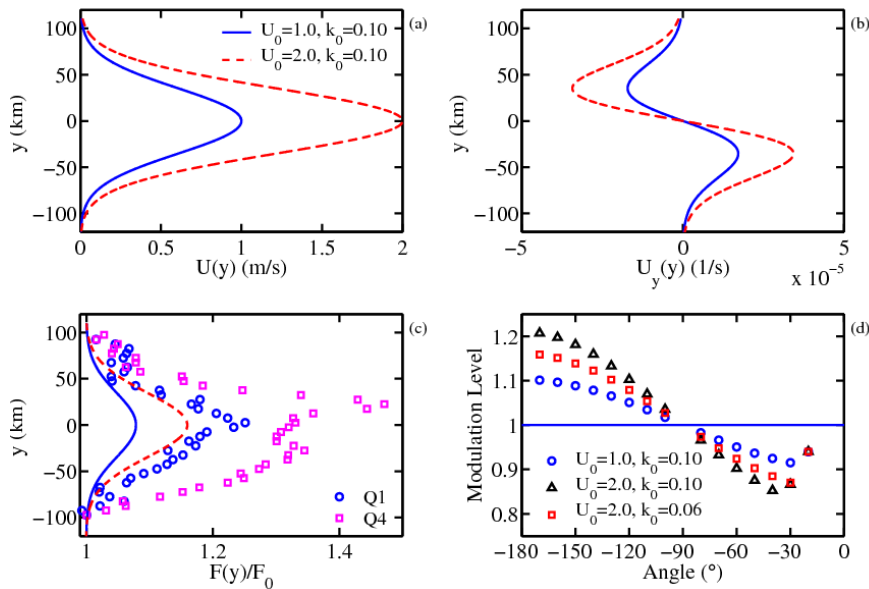


Figure 2. Examples of the modulation computation. (a) Current profile, (b) current shear, (c) distribution of the normalized spectral density across the current, and (d) modulation level as a function of the angle between wave and current. In (c) the altimeter observations of the normalized variance of surface waves (proportional to the square of significant wave height) between 27 and 29°N are superimposed for comparison.